Self-assembled three-dimensional inverted photonic crystals on a photonic chip

Sanna Arpianen, Kevin Vynck, James Dekker, Markku Kapulainen, Worawut
Khunsin, Timo Aalto, Mikael Mulot, Gudrun Kocher-Oberlehrer, Rudolf
Zentel, Clivia M. Sotomayor Torres, et al.

Self-Assembled Three-Dimensional Inverted Photonic Crystals on a Photonic Chip

Sanna Arpiainen*, Kevin Vynck, James Dekker, Markku Kapulainen, Worawut Khunsin, Timo Aalto, Mikael Mulot, Gudrun Kocher-Oberlehrer, Rudolf Zentel, Clivia M. Sotomayor Torres, David Cassagne, and Jouni Ahopelto

Dr. S. Arpiainen, Dr. J. Dekker, M. Kapulainen, Dr. T. Aalto, Dr. M. Mulot, and Prof. J. Ahopelto
VTT Technical Research Centre of Finland, Tietotie 3, B.O. Box 1000, FI-02044 VTT, Finland
E-mail: sanna.arpiainen@vtt.fi
Dr. K. Vynck
Laboratoire Photonique Numérique et Nanosciences (LP2N), UMR 5298, CNRS-IOGS- Univ. Bordeaux, F-33400 Talence, France
Dr. K. Vynck, and Prof. D. Cassagne
Laboratoire Charles Coulomb (L2C), UMR 5221 CNRS-Univ. Montpellier, F-34095 Montpellier, France
Dr. W. Khunsin, Dr. G. Kocher-Oberlehrer, and Prof. C. Sotomayor-Torres
Tyndall National Institute, University College Cork, Lee Maltings, Cork, Ireland
Prof. C. Sotomayor-Torres
ICN2 - Catalan Institute of Nanoscience and Nanotechnology, Campus UAB, 08193 Bellaterra, Spain.
ICREA, Catalan Institution for Research and Advanced Studies, 08010 Barcelona, Spain.
Prof. R. Zentel
Department of Chemistry, University of Mainz, Duesbergerweg 10-14, D-55099 Mainz, Germany

Three dimensional photonic crystals (PhCs) exhibiting a full photonic band gap have high potential in optical signal processing and detector applications. However, the challenges in the integration of the 3D PhCs into photonic circuits have so far hindered their exploitation in real devices. This paper demonstrates the fabrication of 3D PhCs exploiting the capillary directed self-assembly (CDSA) of monodisperse colloidal silica spheres, their inversion to silicon shells, and integration with silicon waveguides. The measured transmission characteristics agree with numerical predictions and provide strong indication of a full photonic band gap in the inverted 3D photonic crystals at wavelengths close to 1.55 µm.

1. Introduction

Photonic crystals have experienced numerous developments and outcomes since their advent in the late 80's.[1,2] The early works focused on 3-dimensional (3D) photonic crystals that promise a full control over the light emission and propagation in space due to complete photonic band gap [3-16]. 3D photonic crystals can provide a route to the realization of very compact photonic devices. The photonic functions typically require embedded single or line defects to control, bend or localize the electromagnetic field inside the crystal. Recently, however, the main emphasis has been on 2-dimensional photonic crystals due to easier fabrication and straightforward integration with planar waveguides,[17-19] though modelling, fabrication and properties of 3-dimensional photonic crystals have also been reported in many papers.[20-27]

3D photonic crystals can be realized in various ways, including mechanical stacking of rod-like structures,[3] lithographic and holographic 3D patterning,[4] focused ion beam (FIB) carving and multidirectional plasma etching.[20-21] For practical photonic circuit applications the challenges are in the scalability to production volumes and, in particular, in the integration with other photonic components.

The approach that is probably the most suitable to large-scale low-cost fabrication of photonic structures is that based on self-assembly of sub-micrometer-sized particles into artificial opals, their subsequent inversion[5,6] and the inclusion of well-defined photonic defects.[5,7-9,22-23] These opals are typically produced by colloidal self-assembly based on gravitational,[10] electrophoretic[11] or vertical sedimentation.[12] Site-selective colloidal self-assembly by micromoulding in capillaries[13] or capillary directed self-assembly (CDSA)[24] combine bottom-up and top-down techniques and have high prospect for controlled large scale fabrication of opals on wafers and their integration into photonic circuits.

Inverted opals can exhibit a full photonic band gap, enabling the design of high-Q optical nanocavities, and slow-light propagation, thereby enhancing the light-matter interaction which

is beneficial to many processes, e.g., photo-oxidation[28] and photoisomerization.[29] The combination of microfluidic channels and inverted photonic crystals with optical access to monitor the evolution of the biological process will have interesting applications in bionanotechnology. The frequency and direction-dependent transmission enables efficient separation of the emitted signal from the exciting mode when characterizing photoemissive processes.[30] In integrated optics the tolerances with respect to lattice order and alignment and to surface quality of the defect lines or defect cavities, combined with the large scale production requirements, are still beyond the reach of the currently available technologies. Utilizing the PhCs as elements in an integrated photonic circuit requires connecting the PhCs to optical waveguides. This major and crucial step has not been achieved so far. In this report we demonstrate integration of inverted 3D opals with silicon ridge waveguides to realise photonic chips. In the fabrication we have used CDSA[24] to build 3D PhCs in predetermined locations on silicon substrate, connected with waveguides to couple light in and out.

2. Sample Fabrication

The process flow for the fabrication of the photonic chips with inverted fcc photonic crystals is shown in **Figure 1**. The structures were patterned on 10 µm thick silicon on insulator (SOI) film by UV lithography and subsequent plasma etching to include both the ridge waveguides and the capillary channels for the directed self-assembly. The waveguides were either defined as 9 µm wide ridges with their surroundings etched 4.5 µm deeper into the SOI film or as 10 µm wide rectangular ribs defined by etching through the SOI film as shown in **Figure 2**. The waveguide cores were covered by a 200-250 nm thick SiO_2 optical cladding and a 20 nm thick alumina (Al_2O_3) film. Al_2O_3 is required to protect the chip during the removal of the silica spheres in the inversion process. Al_2O_3 can be grown conformally with atomic layer deposition (ALD) and it has extremely high selectivity to silicon, 1:80000, in SF_6 based plasma which allows for the efficient removal of excess silicon deposited during the inversion.

Most importantly, after annealing at 900 ℃ for 30 minutes the Al_2O_3 film becomes

chemically resistant to certain hydrofluoric acid (HF) based chemistries that can be used in
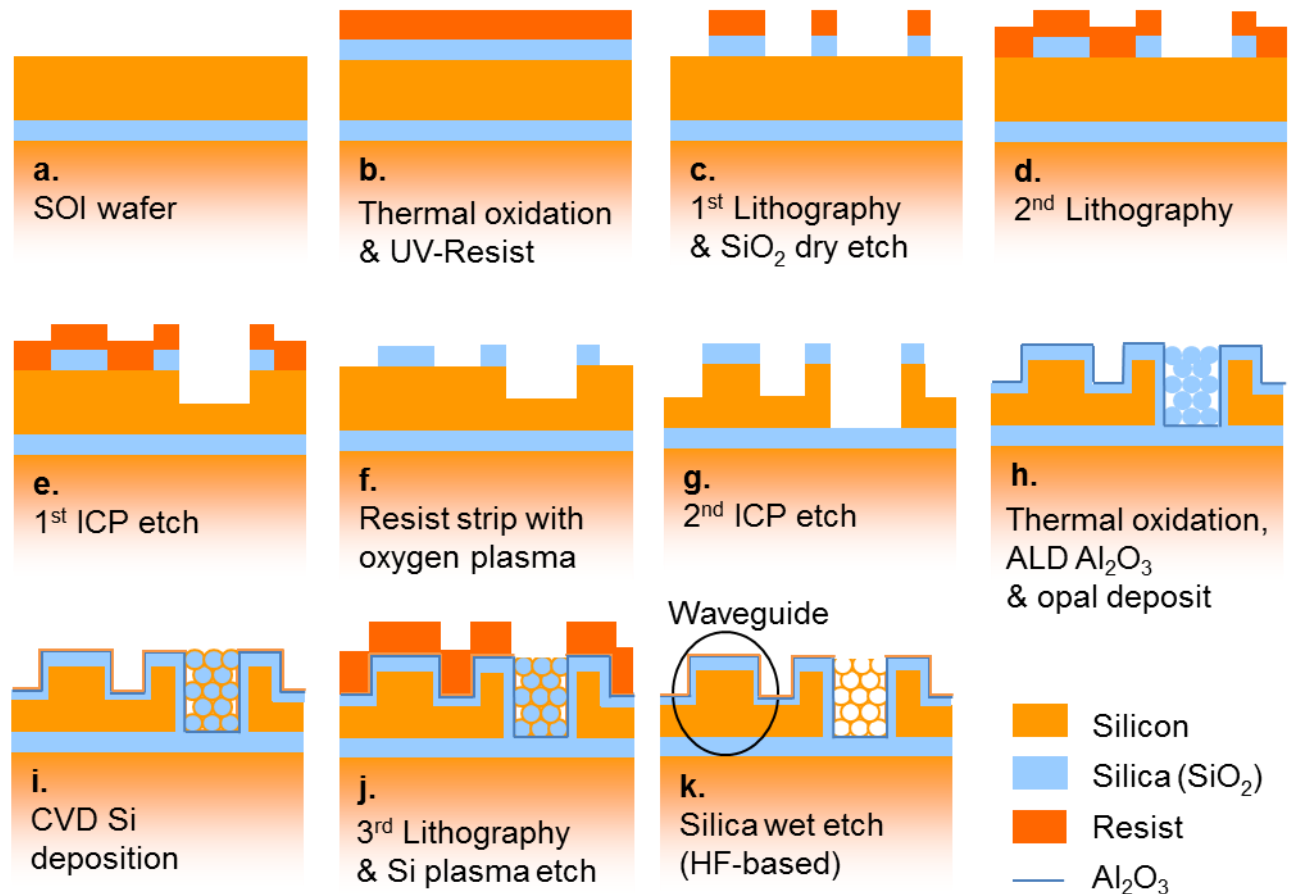
silica sphere removal.

Figure 1. Schematic process flow for the fabrication of inverted photonic crystals on a photonic chip. The SOI wafer (a) is first thermally oxidized (b) and the oxide is patterned to form the hard mask for SOI etch. After patterning a soft polymer mask (d), the deep structures are etched half-way with the first ICP etch (e), the polymer mask is removed with oxygen plasma (f) and the final topography is defined with the second ICP etch (g). The waveguides are thermally oxidized and protected with ALD Al_2O_3 layer, the opals are formed into the cavities with capillary directed self-assembly (h) and a conformal thin silicon film is deposited on all surfaces (i). The top silicon layer is then removed with plasma etch (j) and the silica spheres are removed with HF based wet etch (k).

Artificial opals were deposited from 2–5 vol. % aqueous dispersion of monodisperse colloidal

silica spheres with a diameter of 890 nm synthetized by Unger's method.[27,32] A droplet of

suspension, 0.2–0.8 µL in volume, was dispensed into a reservoir defined on the substrate,

and readily directed via capillary channels into the opal basins. The agglomeration of the

spheres into the basins and their simultaneous self-assembly into face centered cubic (fcc) lattice were driven by solvent evaporation. The opal deposition was performed in a process chamber with 93 % relative humidity and at 30 ℃ temperature. Prior to the opal deposition the substrates were chemically hydrophilized in $NH_4OH:H_2O:H_2O_2$ solution , and an about 40 hour settling time was required to reduce the Al_2O_3 hydrophilicity (amount of surface OH groups) to optimal level for CDSA. Opal deposition on highly hydrophilic Al_2O_3 substrate immediately after the chemical treatment led to uncontrolled spreading of the suspension over the surface, whereas in slightly too hydrophilic substrates the suspension occasionally escaped from the capillary channels and opal basins as shown in Figure 2c. After drying the opal, 100–130 nm thick silicon film was conformally deposited on the structure by low pressure chemical vapour deposition (LPCVD) from silane[5] at 560 °C. During this process the silica sphere diameter reduced to 860 nm as defined from SEM images. The inversion was completed by removal of the silica opal template in a HF based silica wet etch, a dilute mixture of CH_3COOH and NH_4F, that is able to etch SiO_2 selectively against annealed Al_2O_3. Amorphous silicon grown by LPCVD has a high concentration of dangling bonds leading to considerable absorption at near-infrared. Annealing at 600 ℃ transforms the material into polycrystalline phase which is transparent at wavelengths above the fundamental absorption gap of silicon at 1.15 µm. Annealing of LPCVD amorphous silicon at 600 °C has been found to reduce the near-IR attenuation in thin slab waveguides from 42 ± 2 dB/cm to 25 ± 3 dB/cm and additional long heat treatment at 1100 °C and subsequent chemical mechanical polishing (CMP) to further reduce the attenuation down to 10 ± 2 dB/cm[32]. However, in the case of 3D photonic crystals, the surface roughness introduced by the crystallite formation during the high temperature annealing cannot be removed by CMP and crystallization also increases strain that may relax via formation of cracks inside the PhC.
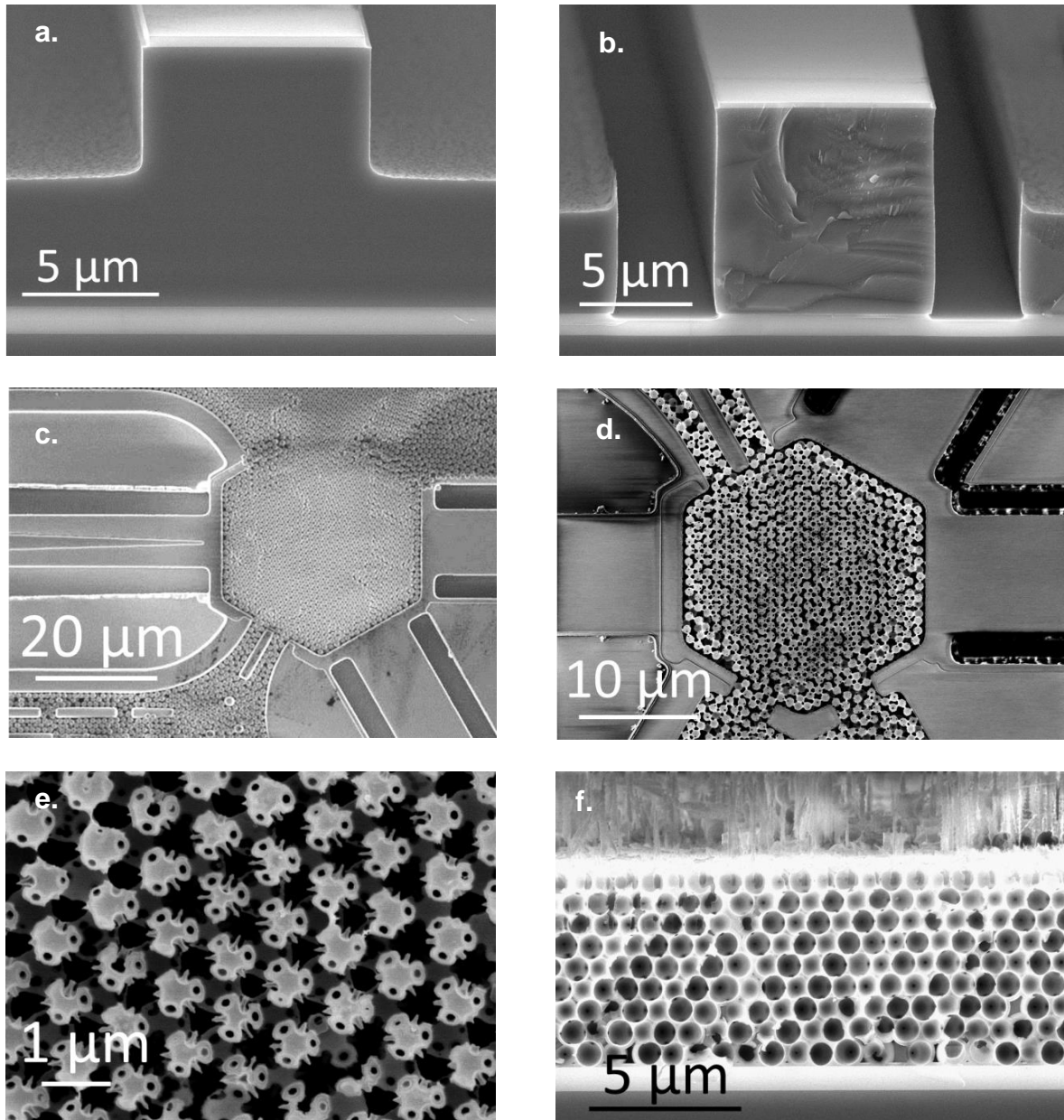
Figure 2. Scanning electron micrographs showing the cross sections of a) the rib and b) the strip waveguides. c) Top view of the integrated opal before inversion. The small overflow of silica spheres illustrates the importance of careful control of the surface properties and is due to too high level of hydrophilicity of the Al_2O_3 surface during the opal self-assembly. d,e) Top views of the silicon inverted opals show the fcc arrangement. The partial destruction of the topmost silicon shells results from the removal of the thick silicon grass, still visible in the cross section image f) of a typical inverted opal.

3. Modeling and simulations

The behaviour of incident light at the waveguide – PhC interface was simulated by the 3D finite-differential time-domain (FDTD) method using the freely available software package MEEP[33]. The band structure of the inverted opals was calculated with the MIT Photonics-

Bands[34] that computes the fully-vectorial eigenmodes of Maxwell's equations with periodic boundary conditions in a planewave basis.

The FDTD simulations were performed for a 4–5 µm long PhC interposed by waveguides with height and width of 3 µm. The 3D PhC was defined as a face centered cubic (fcc) lattice of air spheres with diameter d, embedded in a silicon background as shown in **Figure 3**. The normalized frequency a/λ is related to the lattice dimensions as a $= d\sqrt{2}$. For simplicity, the spheres were cut at the side interfaces, otherwise maintaining the fcc arrangement. In addition, the air necks between the spherical voids and the finite silicon shell thickness around them were not included into the model. The silicon fill factor results in significant changes in the spectral width and position of the photonic band gap, yet the purpose of FDTD simulations here is to get insight into the origin of the spectral features observed experimentally rather than making a quantitative comparison. The fcc lattice was oriented according to the experimental arrangement, with (111) plane at the surface and (110) planes perpendicular to the waveguide end facets. The direction of the mode propagation is thus parallel to both of these high symmetry planes. The planes perpendicular to the mode propagation (parallel to the waveguide end facets) define a reciprocal lattice point M located in the mid-point of the line combining the L and the U high symmetry points. Silicon was treated as dielectric with frequency independent refractive index (n = 3.45), which is adequate at near infrared wavelengths above the optical absorption gap tail at 1.15 µm.
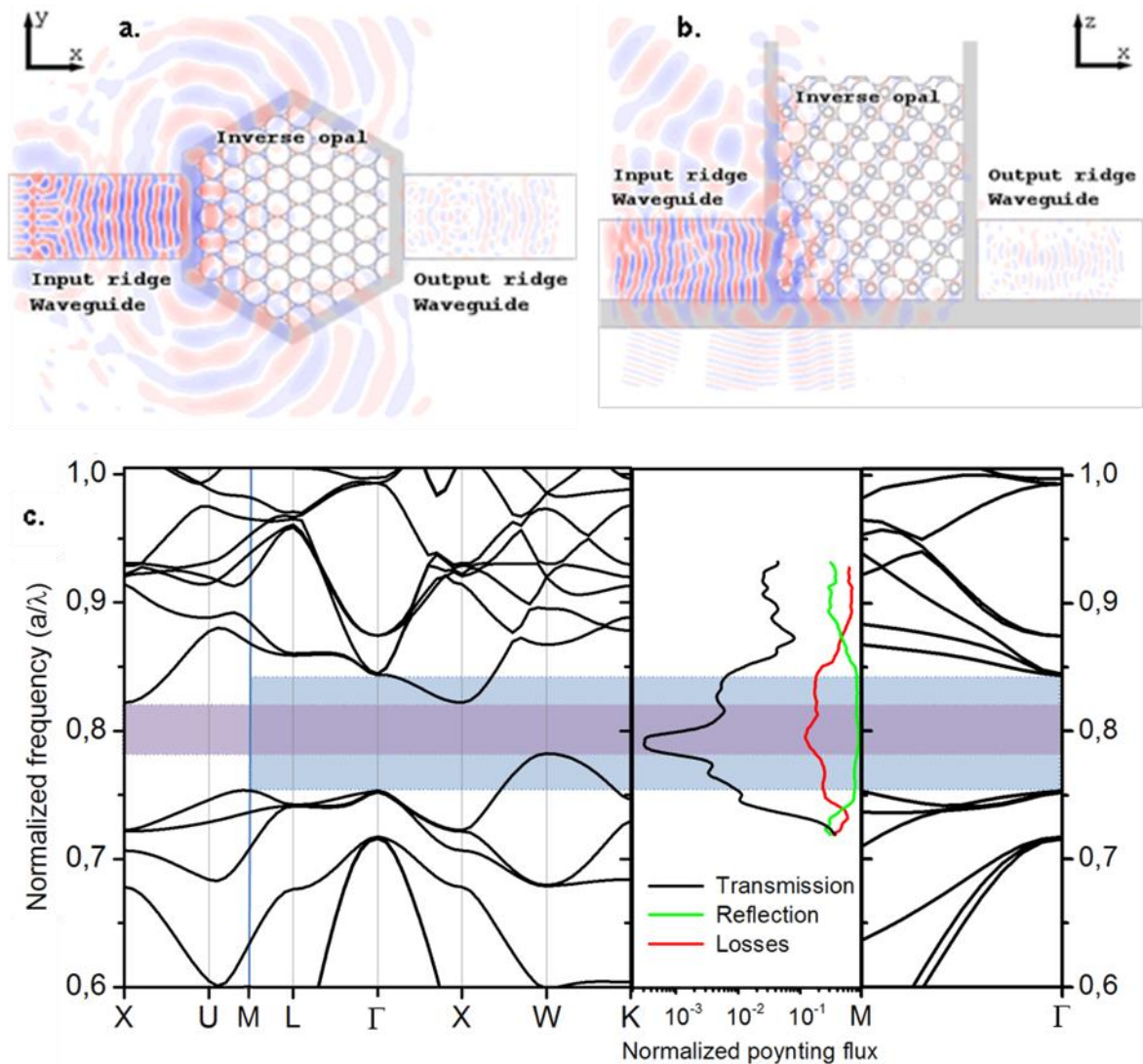
Figure 3. 3 FDTD and band structure simulations with a fully filled silicon inverse opal. a) Top view and b) side view of a continuous TE-polarized wave traveling via a 3 µm by 3 µm strip waveguide through a 5 µm wide hexagonal well containing the PhC. The photon energy in the simulation corresponds to the mid band gap energy. c) Calculated band structure and simulated transmitted and reflected spectra for the corresponding structure. The full band gap at $0.78 < a/\lambda < 0.82$ induces high reflection and corresponding reduction in the transmitted intensity. The effect of the pseudo gap in ΓM direction at $0.76 < a/\lambda < 0.84$ is similar, but not as strong.

The simulated field intensity distribution illustrates the behavior of a continuous wave

reaching the interface between the waveguide and PhC at a wavelength in the middle of the

photonic band. The light is clearly stopped by the inverse opal, but the decrease in

transmission is not complete as the light reflected by the inverted opal is partially coupled into

the silicon walls and substrate where it propagates and reaches the output ridge waveguide, as

can be seen in Figures 3a and 3b. The simulated transmission and reflection spectra are directly related to the photonic band structure[34] of the inverted opal as illustrated in Figure 3c. In the FDTD simulation, the full photonic band gap (PBG) of the inverse opal is observed as a clear dip in transmission, accompanied by a smaller decrease in the range of the pseudo gap in ΓM direction.

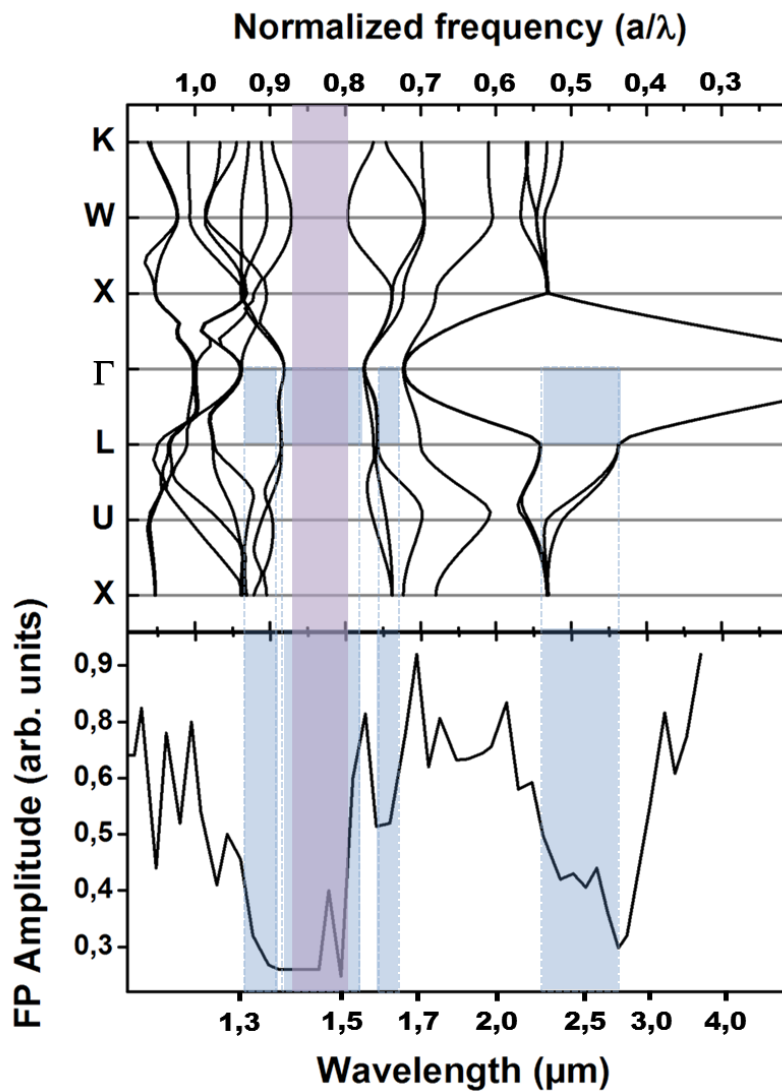**Figure 4.** Optical analysis of the inverted 3D PhC interposing ridge waveguides. a) Simulated band structure of inverted fcc crystal constructed from thin silicon shells as in the experiment. b) Normalized Fabry-Perot amplitude of the reflected IR light as measured from top of the PhC in ΓL direction. The pale blue regions indicate pseudo gap position in ΓL direction and the violet region indicates the full photonic band.

4. Optical and structural characterization

The fabricated inverted photonic crystals were analysed by scanning electron microscopy as shown in Figures 2d–f. The band structure of the experimental inverted opals in **Figure 4**a was defined according to the dimensions measured from the SEM images, the silicon shell being 100 nm and the holes between the spheres roughly 60 nm. The location of these holes in Figure 2e also clearly indicates the fcc arrangement instead of the less favourable hcp. Optical analysis was made by infrared reflection spectroscopy from the top of the inverted opal in ΓL direction and by measuring the transmission through the waveguide in ΓM direction.

The transmission characteristics measured from the top of the inverted opal are shown together with the calculated photonic band structure in Figure 4. The experimental data is based on reflection spectra measured with an IR microscope from the top surface of the inverted opals. Due to the roughness of the inverted PhC surface and the spot size exceeding the PhC dimension, only small part of the total intensity of the spectra was reflected from the top surface of the inverted opal and thus the PhC reflection could not be directly extracted from the measured data.

However, the Fabry-Perot oscillations originating from multiple reflections between the top and the bottom interfaces of the 10 µm thick PhC were clearly distinguishable. The amplitude of these oscillations is proportional to the interface reflectivity and PhC transmittance and allows extraction of the transmission characteristics in ΓL direction perpendicular to the substrate surface. The contributions from the PhC top surface reflection and from the simultaneous low frequency Fabry-Perot oscillations through the buried oxide (BOX) film between the PhC and the silicon handle wafer were excluded by normalising each amplitude with the average reflection amplitude. As shown in the Figure 4, at the photon energies in range of full photonic band gap ($a/\lambda = 0.8$–0.87 or $\lambda = 1.4$–1.53 µm) there is a drastic decrease in the amplitude, extending over the adjacent pseudo gaps between the 11th and 12th

bands and 5th and 6th bands, thus covering the range from 1.3 to 1.65 µm. The amplitude is

also strongly reduced near the position of the first order pseudo gap (a/λ = 0.43–0.54, λ = 2.2–
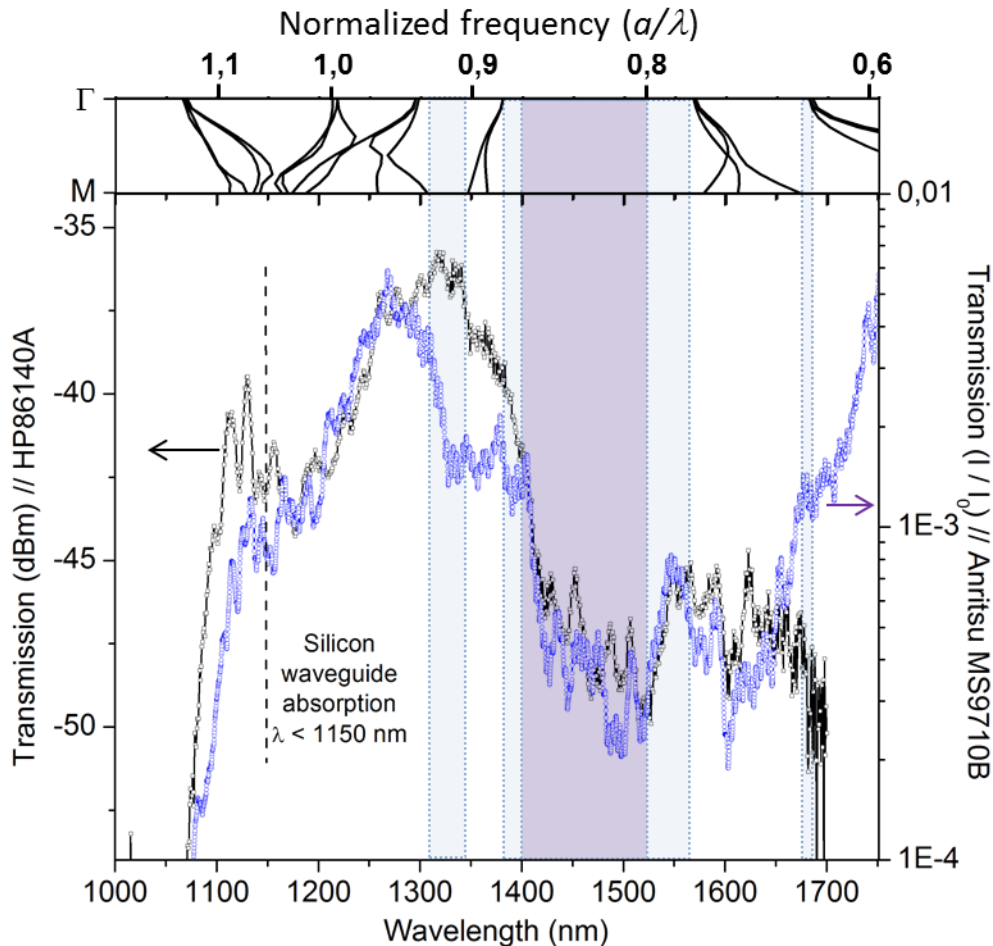
2.9 µm) in the ΓL direction.

Figure 5. Transmission spectra measured through the waveguides coupled to the photonic crystal. The measurement was carried out with two different spectral analyzers to determine which spectral features are due to the non-linear dynamic response of the analyser and which are due to the sample. Pale blue colours indicate the pseudo gaps in ΓM direction and violet corresponds to the full photonic band gap defined at W point as presented in Figure 4.

The transmission through the waveguide – PhC – waveguide structure shown in **Figure 5** was

measured by end coupling the incident light from a single mode optical fiber into the

waveguide. White light supercontinuum laser was used as the light source, as it offers a wide

spectral range from 600 to 1800 nm with high intensity that is optimal for probing the band

structure of embedded PhCs.

The transmission spectra in Figure 5 show the silicon absorption below 1.15 µm and a 5 dBm reduction in the transmitted intensity from 1.4 to 1.53 µm, corresponding to the spectral position of the full photonic band gap at reduced frequencies of $a/\lambda = 0.8$–0.87, similar to the simulated fully infiltrated PhC in Figure 3. In the partially filled PhC the full band gap is wider than in the simulated structure and thus the effect of the pseudo gap in the direction of mode propagation (ΓM) overlap the band gap. The reduction in the transmitted intensity, assumed to correspond the ΓM pseudo gap in the simulated structure, can however be seen also in the measured spectrum, with spectral range of 1.3 µm to 1.65 µm exactly corresponding to the three pseudo gaps in the ΓL direction.

5. Discussion

Even though the wider region in the FDTD simulation also corresponds to the pseudo gap in ΓL direction, the origin of these spectral features is probably different. In the simulation the lattice is perfect, and the reduction is mainly due to reflection which is close to unity across the whole range of interest. In the real structure, scattering from defects and surface roughness is likely to play an important role, smearing out the narrow pseudogaps and enabling light to couple and propagate along allowed directions (e.g. ΓU or ΓW), thereby reducing the actual amount of light that is transmitted through the PhC. Furthermore, it is known that small imperfections on periodic PhCs can lead to light localization phenomena,[2,35] which would result in a drastic reduction of the light transmission. Investigating the effect of disorder on light propagation in our integrated inverted opals is clearly beyond the scope of this work but it should be addressed carefully in the future.

6. Conclusion

To conclude, we have reported the first realization of 3D PhC fabricated by self-assembly, coupled to ridge waveguides in a photonic circuit. Simultaneous measurement of the band gap from ΓL and ΓM directions and comparison with numerical simulations verifies both the fcc

order of the lattice and the existence of the band gap in the integrated 3D PhC near the operating telecommunication wavelength (1.55 µm). While this work constitutes an important step towards the use of 3D inverse opal PhCs in integrated optics, it also emphasizes issues that need to be addressed in future works, namely the light coupling to the substrate and surrounding structures such as the walls of the PhC basin, as well as the structural imperfections, which result in losses in the transmission and reflection.

7. Experimental Section

Photonic chip fabrication and opal deposition: Bonded silicon on insulator (SOI) wafers with a 10 µm thick (100) SOI film (5 Ω-cm) on a 1 µm thick buried oxide (BOX) were patterned into a photonic chip as described elsewhere.[24] A 200–250 nm thick SiO_2 film was grown by dry oxidation at 900 ℃ and covered with a 20 nm Al_2O_3 film by ALD from trimethylaluminium (TMA) and water at 300 ℃ and annealed at 900 ℃ for 30 minutes. The wafers were covered with protective resist (AZ5214e), diced and the chip edges were polished with a diamond paste. After resist removal, Al_2O_3 was hydrophilized in $NH_4OH:H_2O:H_2O_2$ 1:5:1 at 65 ℃ for 5–10 minutes and rinsed in de-ionized water. After 40 hours settling in air, a 0.2–0.8 µl droplet of 2–5 vol. % aqueous dispersion of 890 nm silica spheres was dispensed into a reservoir on the substrate. The suspension was directed via capillary channels into opal basins in a process chamber with 93 % relative humidity of the solvent (water) and 30 ℃ temperature.

Inversion: 100–130 nm of amorphous silicon was deposited by SiH_4 decomposition at 560 ℃. The silica spheres were removed in $CH_3COOH:NH_4F(40\%):H_2O$ 1:1:1 solution, after which the hazardous etch residues were rinsed in de-ionized water for 40 minutes. Silicon was crystallized by annealing in nitrogen ambient at 600 ℃ for 2–16 hours and some of the samples further at 900 ℃ for 2 hours.

Measurements: Reflected spectrum from the top of the PhC was measured with Bruker FTIR spectrometer equipped with a microscope using 15X lens with NA=0.4, working distance 25 mm and acceptance (half angle) 15 degrees.

The intense broad spectrum used in transmission measurements (via waveguides) was based on photonic crystal supercontinuum, generated by coupling the 1064 nm output radiation from a miniature Q-switched Nd-YAG laser into a highly non-linear photonic crystal fiber. The result is a broadband spectrum extending from 600 to 1800 nm with an approximately -15 dBm/nm output power. The supercontinuum light was coupled into a single mode photonic fiber, which was aligned with the ridge waveguide. Light coupling into the waveguide was monitored by detecting the mode profile at the waveguide output with a CCD IR camera and scattering from the vicinity of the PhC. The transmission spectra was found to depend strongly on the input fiber alignment since the waveguides were not truly single mode, but able to support a multitude of modes with only one properly confined into the ridge waveguide core. However, when properly aligned, the shape of the output signal was elliptical, with FWHM width of 7 µm and height 5 µm, respectively. The measurement configuration was complemented with a multimode optical fiber coupled to the waveguide end, and the transmitted intensity was recorded with optical spectrum analysers (OSAs). Because the difference between the transmitted intensity and the reference was larger than the dynamic range of the OSAs, two different analysers, HP 86140A and Anritsu MS9710B, with different intensity distortion were used to confirm the main features of the spectra.

Received: ((will be filled in by the editorial staff))
Revised: ((will be filled in by the editorial staff))
Published online: ((will be filled in by the editorial staff))

[1]   E. Yablonovitch, *Phys. Rev. Lett.* **1987**, *58 (20)*, 2059.

[2]   S. John, *Phys. Rev. Lett.* **1987**, *58 (23)*, 2486.

[3]   S. Y. Lin, J. G. Fleming, D. L. Hetherington, B. K. Smith, R. Biswas, K. M. Ho, M. M. Sigalas, W. Zubrzycki, S. R. Kurtz, J. Bur, *Nature* **1998**, *394*, 251.

[4]   V. Berger, O. GauthierLafaye, E. Costard, *J. Appl. Phys.* **1997**, *82*, 60.

[5]   Y. A. Vlasov, X.-Z. Bo, J. C. Sturm, D. J. Norris, *Nature* **2001**, *414*, 289.

[6]   A. Blanco, E. Chomski, S. Grabtchak, M. Ibisate, S. John, S. W. Leonard, C. Lopez, F. Meseguer, H. Miguez, J. P. Mondia, G. A. Ozin, O. Toader, H. M. van Driel, *Nature* **2000**, *405*, 437.

[7]   F. Jonsson, C. M. Sotomayor Torres, J. Seekamp, M. Schniedergers, A. Tiedemann, J. Ye, R. Zentel, *Microelectron. Eng.* **2005**, *429*, 78.

[8]   V. Lousse, S. Fan, *Opt. Express* **2005**, *14*, 866.

[9]   D. L. C. Chan, E. Lidorikis, J. D. Joannopoulos, *Phys. Rev. E* **2005**, *71*, 056602.

[10]   K. E. Davis, W. B. Russel, W. J. Glantschnig, *Science* **1989**, *245*, 507.

[11]   M. Trau, D. A. Saville, I. A. Aksay, *Science* **1996**, *272*, 706.

[12]   P. Jiang, J. F. Bertone, K. S. Hwang, V. L. Colvin, *Chem. Mater.* **1999**, *11*, 2132.

[13]   H. Míguez, S. M. Yang, N. Tétreault, G. A. Ozin, *Adv. Mater.* **2002**, *14*, 1805.

[14]   C. Lopez, *Adv. Mater.* **2003**, *15*, 1679.

[15]   P. Braun, S. Rinne, F. García-Santamaría, *Adv. Mater.* **2006**, *18*, 2665.

[16]   A. Chutinan, S. John, O. Toader, *Phys. Rev. Lett.* **2003**, *90*, 123901.

[17]   M. Notomi, A. Shinya, K. Yamada, J.-I. Takahashi, I. Yokohama, *IEEE J. Quantum Electron.* **2002**, *38 (7)*, 736.

[18]   A. Talneau, P. Lalanne, M. Agio, C. M. Soukoulis, *Opt. Lett.* **2002**, *27 (17)*, 1522.

[19]   E. Chow, S. Y. Lin, S. G. Johnson, P. Villeneuve, J. Joannopoulos, J. Wendt, G. Vawter, W. Zubrzycki, H. Hou and A. Alleman, *Nature* **2000**, *407*, 983.

[20]   K. Suzuki, K. Kitano, K. Ishizaki, S. Noda, *Opt. Express* **2014**, *22 (14)*, 17099.

[21]   J. M. van den Broek, L. A. Woldering, R. W. Tjerkstra, F. B. Segerink, I. D. Setija, W. L. Vos, *Adv. Funct. Mater*. **2011**, *22*, 25.

[22]   S. Rinne, F. Garcia-Santamaria, P. Braun, *Nat. Photonics* **2008**, *2*, 52.

[23]   G. Qiu, K. Vynck, D. Cassagne, E. Centeno, *Opt. Express* **2007**, *15*, 3502.

[24]   S. Arpiainen, F. Jonsson, J. R. Dekker, G. Kocher, W. Khunsin, C. M. Sotomayor Torres, J. Ahopelto, *Adv. Funct. Mater*. **2009**, *19 (8)*, 1247.

[25]   L. A. Woldering, A. Mosk, W. L. Vos, *Phys. Rev. B* **2014**, *90*, 115140.

[26]   K. Ishizaki, M. Koumura, K. Suzuki, K. Gondaira, S. Noda, *Nat. Photonics* **2013**, *7*, 133.

[27]   J. H. Ye, R. Zentel, S. Arpiainen, J. Ahopelto, F. Jonsson, S. G. Romanov, C. M. Sotomayor Torres, *Langmuir* **2006**, *22 (17)*, 7378.

[28]   a) J. Zhao, X. Yang, *Building and Environment* **2003**, *38 (5)*, 645; b) J. Herney-Ramirez, M. A. Vicente, L. M. Madeira, *Appl. Catal., B* **2010**, *98 (1–2)*, 10.

[29]   M. Kaur, A. K. Srivastava, *J. Macromol. Sci., Part C: Polym. Rev.* **2002**, *42 (4)*, 481.

[30]   E. R Goldman, A. R Clapp, G. P. Anderson, H. T. Uyeda, J. M. Mauro, I. L. Medintz, H. Mattoussi, *Anal. Chem.* **2004**, *76 (3)*, 684.

[31]   K. Unger, H. Giesche, J. Kinkel (Merck Patent GmbH), German Patent DE 35 34143A, 1985.

[32]   a) L. Liao, D. Lim, A. Agarwal, X. Duan, K. Lee, L. Kimerling, *J. Elect. Mat*. **2000**, *29 (12)*, 1380; b) A. Säynätjoki, S. Arpiainen, J. Ahopelto, H. Lipsanen, *Proc. Int. Conf. Phys. Semicond., 27th*, **2004**.

[33]   A. Oskooi, D. Roundy, M. Ibanescu, P. Bermel, J. D. Joannopoulos, S. G. Johnson, *Comput. Phys. Commun*. **2010**, *181*, 687.

[34]   S. Johnson, J. Joannopoulos, *Opt. Express* **2001**, *8 (3)*, 173.

[35]   C. Conti, A. Fratalocchi, *Nat. Phys.* **2008**, *4*, 794.

Scalable fabrication process of integrated 3D photonic crystals, based on a directed self-assembly of colloidal opals, is demonstrated. The propagation and loss characteristics of the photonic crystal, as probed both via the integrated waveguides and perpendicular to the top surface, agree with the FDTD simulation and indicate the existence of a full photonic band gap at around 1.55 µm.

Keywords integration; inverted opals; photonic band gap; photonic crystals; waveguides

S. Arpiainen*, K. Vynck, J. Dekker, M. Kapulainen, W. Khunsin, T. Aalto, M. Mulot, G. Kocher-Oberlehrer, R. Zentel, C. M. Sotomayor Torres, D. Cassagne, J. Ahopelto

Self-Assembled Three-Dimensional Inverted Photonic Crystals on a Photonic Chip

ToC figure